Utkal University Journal of Computing & Communications,
Vol. 1, Issue. 2 (2023) *e-ISSN:2584-203X*

Transforming Retinal Image Analysis: Bilinear Filter for Blood Vessel Extraction

Deepak Kumar Maharana[1][0000-0002-5514-5675], Pranati Das[2]

[1,2]IGIT Sarang, BPUT, Dhenkanal, Odisha, 759146, India

deepakkumarmoharana@gmail.com, daspranati@yahoo.co.in

Abstract: Accurate segmentation of retinal vasculatures is a vital job required for the identification of a range of clinical disorders. This paper introduces an efficient system for retinal vasculature segmentation. The retinal image undergoes pre-processing through a unique fusion of CLAHE and a homomorphic filter. Bilateral filtering is used in blood vessel segmentation to improve contrast and minimize noise in retinal pictures. Furthermore, a unique thresholding approach called Otsu with entropy thresholding is used for segmentation. At the post-processing phase, the resultant image is generated through the utilization of morphological cleaning and an area-based thresholding approach. The suggested approach's efficacy is evaluated using the DRIVE and STARE datasets, and its outcomes are benchmarked against current methodologies.

Keywords: CLAHE, Homomorphic Filtering, bilateral filtering, Entropy Otsu Thresholding

1. Introductıon

Retinal images hold substantial importance in the field of medical imaging technology. Prompt diagnosis is critical in sight-threatening disorders such as hypertension, stroke, diabetic retinopathy, and glaucoma, that can ultimately cause blindness. Diabetes is a substantial global issue, with the International Diabetes Federation estimating that the worldwide diabetic population reached 463 million in 2019. Without preventive measures, this number is anticipated to rise to 700 million by 2045 [1]. As a result, retinal image analysis has risen to prominence as a major diagnostic technique in modern ophthalmology. Neovascularization can be used to identify diabetic retinopathy, which is essential for averting major health consequences. But precisely identifying these minute anomalies is extremely difficult. Although manually separating data is a possibility, it is hard, difficult, and highly susceptible to mistakes. Consequently, there has always been a strong emphasis on developing automated techniques for extracting the retinal vasculature. Many researchers have developed different ways to segregate the vascular regions from the background. Several methodologies have been suggested for blood vessel segmentation, including supervised strategies, unsupervised strategies, and various others, often leveraging various databases for experimentation [2]. In a supervised strategy, features are derived from individual pixels in the retinal image. These features, along with manually labelled ground truth images from the database, are used to train a classifier through supervised learning. The resulting vascular extraction method divides the pixels of the retinal photograph into two

✉ deepakkumarmoharana@gmail.com

distinct classifications: vessel pixels and non-vessel pixels. The subsequent classifiers represent a few of those applied in the supervised approach: neural network (NN) [3], ensemble classifier [4], Bayesian model [5], Gaussian mixture model (GMM) [6], and extreme learning [7]. support vector machine (SVM) [8], Ada-boost [9], etc. On the other hand, the unsupervised strategy achieves retinal vasculature delineation in an image without relying on classifier training. This strategy is more economical in terms of computing. The unsupervised method utilizes several types of techniques, including matched filtering [10–11], morphological approaches [12], and model-based approaches [13]. The current work introduces an unsupervised scheme for segmenting retinal vasculatures. Reviewing the literature reveals that there are many different ways to separate blood vessels. These techniques, meanwhile, are sometimes time-consuming and difficult to use. Therefore, the recent work is concentrated on the creation of an effective blood vessel extraction technique with the objective of reducing time requirements and optimizing the procedure for uncomplicated adoption.

The study's remaining portion follows this structure: Section 2 contains the proposed methodology; Section 3 includes the results; and Section 4 presents the conclusion of the study.

2. Methodology

While numerous methods have been put forth to extract vascular structures from the retinal image, and each publication claims superior performance compared to its counterparts, the process of blood vessel extraction remains a formidable task. In this work, we provide a three-step procedure. In the primary stage, the photograph is pre-processed by implementing the Contrast Limited Adaptive Histogram Equalization (CLAHE), homomorphic filter, and bilateral filter. The retinal vasculatures are then extracted using Otsu entropy thresholding, and excess noise is then removed by applying pixel-based thresholding. Fig. 1 represents the model for the proposed work.

2.1. Pre-processing

There is frequently poor illumination of blood vessels because it is difficult to capture retinal images through the pupil. Due to the low contrast that results, it is challenging to detect vessels in darker areas. As a result, maximizing the extraction of fine vessels depends greatly on the pre-processing processes. Therefore, enhancing the overall image quality through an efficient pre-processing stage is crucial. Blood vessels and other anatomical structures in the retina often contain a good balance of information in the green channel. By complementing the green channel, it essentially inverts the pixel values, which can help highlight blood vessels against the background. This process can improve the contrast and make it easier for segmentation algorithms to precisely identify and isolate the vascular structures.

2.2. CLAHE (Contrast Limited Adaptive Histogram Equalization)

In the preliminary stage of image enhancement, we employ CLAHE [14]. This process involves partitioning the entire image into uniform-sized regions. We implement CLAHE within each of these regions to enhance the contrast. The operator sets a clip limit that evenly spreads out the gray-level values across the photograph, effectively boosting the visibility of delicate vessels. These vessels may not be clearly discernible in a green channel image.

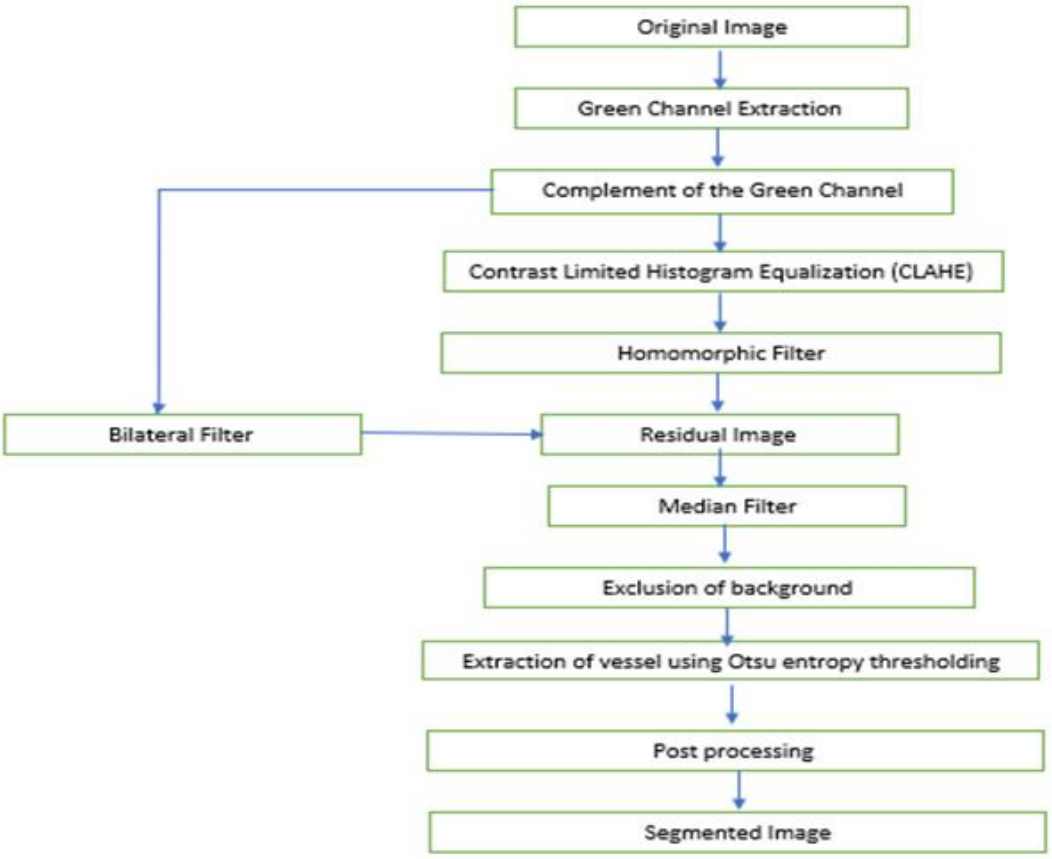

Fig. 1. Proposed Model

2.3. Homomorphic Filter

The primary purpose of a homomorphic filter [15] is to improve the clarity and visibility of fine details in images affected by irregular or non-uniform illumination. In mathematical terms, an image can be expressed as the product of its illumination L (x, y) and reflectance R (x, y), which can be represented as

$$I(x,y) = L(x,y) * R(x,y) \quad (1)$$

The homomorphic filtering process typically involves five stages:

Stage 1: Apply a logarithmic function to convert multiplicative components into additive components.

$$z(x,y) = \ln L(x,y) + \ln R(x,y) \quad (2)$$

Stage 2: Conduct a Fourier transform of the image for frequency domain transformation.

$$Z(u,v) = F_L(u,v) + F_R(u,v) \quad (3)$$

Stage 3: Process the resulting transformed image using a filter function.

$$S(u,v) = H(u,v)\, F_L(u,v) + H(u,v)\, F_R(u,v) \quad (4)$$

Stage 4: Generate the filtered image in the spatial domain by performing an inverse Fourier transform.

$$s(x,y) = F^{-1}(S(u,v)) \quad (5)$$

Stage 5: Finally, apply the exponential function to reverse the log transform and obtain the enhanced image.

$$g(x, y) = \exp(s(x, y)) \quad (6)$$

2.4. Bilateral Filtering

In medical image analysis, edges serve as critical features of interest. Therefore, an edge preservation technique is employed to both diminish noise and retain edge details while achieving smoothing. Among the different types of edge preserving filters bilateral filter [16] is one of them. Bilateral filtering is a method that operates locally and non-linearly without requiring iterative processes. It takes into account both the similarity in gray levels (or colors) and the spatial proximity of neighboring pixels. The bilateral filter's output may be calculated mathematically as follows for pixel position p:

$$I_{BLF}(p) = \frac{1}{w}\sum_{q\in S} G_{\sigma_s}(\|p - q\|)G_{\sigma_r}(|I(p) - I(q)|)I(q) \quad (7)$$

Here $G_{\sigma_s}\|p - q\|) = e^{-\frac{p-q^2}{2{\sigma_s}^2}}$ is a geometric closeness function.

$G_{\sigma_r}(|I(p) - I(q)|) = e^{-\frac{|(Ip-Iq)|^2}{2{\sigma_r}^2}}$ is a gray-level similarity function.

$W = \sum_{q\in S} G_{\sigma_s}(\|p - q\|)G_{\sigma_r}(|I(p) - I(q)|)$ is used as a constant for normalization.

The behaviour of the bilateral filter is influenced by the two parameters, σ_s and σ_r. In this case $\sigma_s = 3$ and $\sigma_r = 0.1$ is taken. Tables 1 and 2 show that using $\sigma_s = 3$ and $\sigma_r = 0.1$ yields higher specificity and accuracy in both the DRIVE and STARE datasets. Though the average sensitivity reduces significantly compared to $\sigma_s = 3$ and $\sigma_r = 0.05$, it still remains fair.

Table 1. Variation of Average Sensitivity, Specificity, and Accuracy W.R.T. Different Values σ_s and σ_r for the DRIVE Database

σ_s	σ_r	Sen	Spec	Acc
1	0.01	0.67592	0.98074	0.953795
1	0.05	0.679835	0.97616	0.94993
1	0.1	0.680135	0.98066	0.95413
3	0.01	0.6963	0.9771	0.9523
3	0.05	0.7149	0.9776	0.9535
3	0.1	0.6948	0.9814	0.9546

Table 2. Variation of Average Sensitivity, Specificity and Accuracy w.r.t. Different Values σ_s and σ_r For STARE Database

σ_s	σ_r	Sen	Spec	Acc
1	0.01	0.696965	0.9619	0.94142
1	0.05	0.699905	0.9683	0.942485
1	0.1	0.698545	0.9639	0.943375
3	0.01	0.70344	0.957	0.93735
3	0.05	0.727595	0.959	0.94116
3	0.1	0.7244	0.9653	0.9438

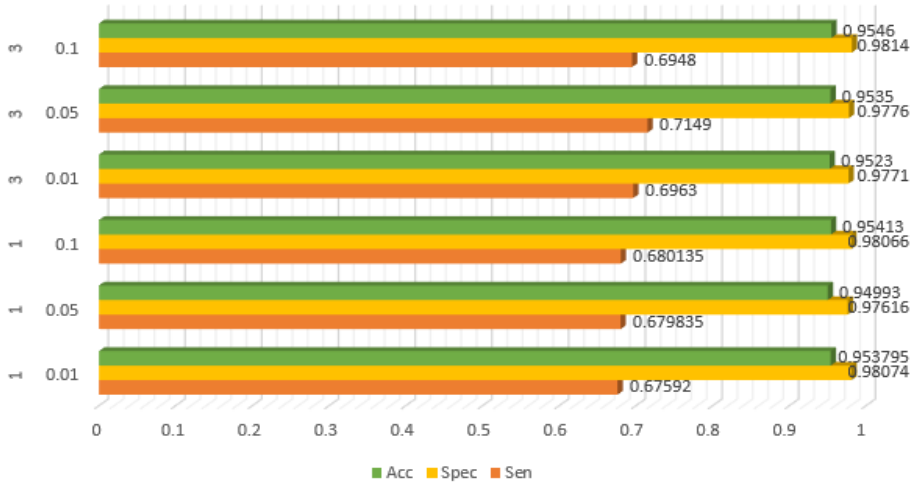

Fig. 2. Performance Analysis of Different Values σ_s and σ_r For the DRIVE Database

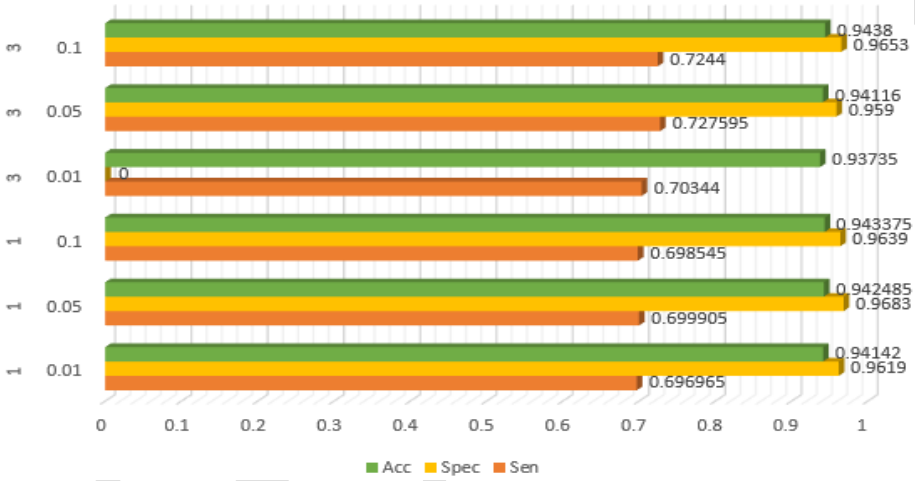

Fig. 3. Performance Analysis of Different Values σ_s and σ_r For the STARE Database

2.5. Background Exclusion

The residual image is defined as the difference between the homomorphic filter output and the bilaterally filtered output. We apply a morphological opening operation to the residual image. We implement a median filter to reduce the noise. The morphologically opened image, obtained by using a disk structuring element, is subtracted from the median-filtered output to obtain the background excluded output. Fig. 4 displays the results of image preprocessing, which include the original image, the green channel image, the green channel image's complement, the image after CLAHE, the homomorphic filtered image, the bilateral filtered image, and the background excluded image.

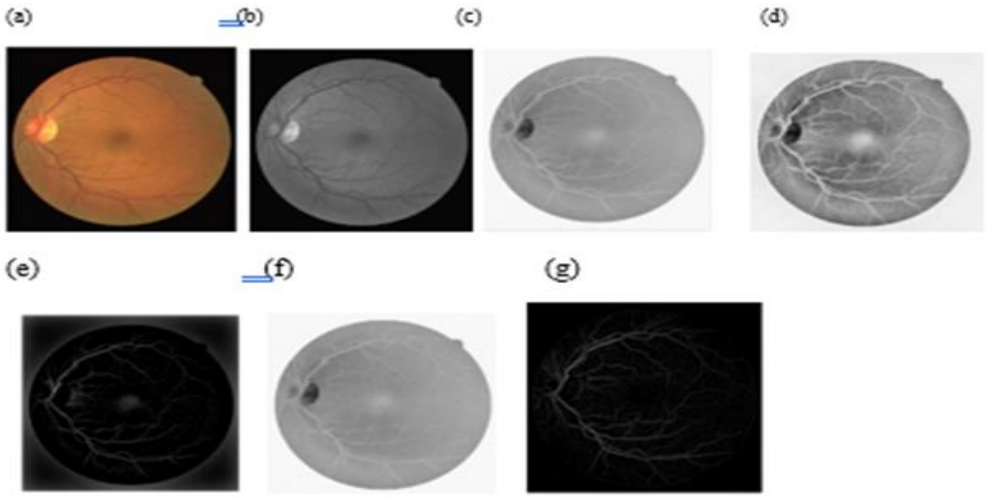

Fig.4. (A) Original Image (B) Green Channel Image (C) Complement Of Green Channel Image (D) Image After CLAHE Operation (E) Homomorphic Filtered Image (F) Bilateral Filtered Image (G) Background Excluded Image.

2.6. Vasculature Extraction using Otsu Entropy Thresholding

In order to characterize an attribute of an image, one can employ entropy as a statistical measure. When an image consists of a prolonged sequence of pixels with similar intensity values, it results in a small value of entropy. Conversely, if a lengthy sequence of pixels in an image share the same gray-level values, the entropy is reduced to zero. In this suggested approach, the entropy [18] may be computed by specifying a gray-value k. "Posteriori of an image is defined by [18]".

$$H_n' = -P(k)lnP(k) - (1 - P(k))\ln(1 - P(k)) \quad (8)$$

$$\text{Where } (k) = \sum_{i=0}^{k} p(i), \sum_{i=k+1}^{M-1} p(i) = 1 - p(k) \quad (9)$$

We get an insignificant outcome if we optimize H_n'.

$$P(k) = 1 - P(k) = 0.5$$

An objective function is implemented to solve this issue and it is denoted by [18].

$$\varphi(k) = \ln P(k)(1 - P(k)) + \frac{H_k}{P(k)} + \frac{H_n - H_k}{1 - P(k)} \quad (10)$$

$$\text{Where } H_k = -\sum_{i=0}^{k} P(i)\ln P(i), H_n = -\sum_{i=0}^{M-1} P(i)\ln P(i) \quad (11)$$

"As a threshold value, the gray value k, which maximizes φ(k), should be used, since it maximizes the image's distinction between background and foreground" [11]. "However, if the distributions of the foreground and background are uniform then eq. (9) equivalent to

$$\varphi(k) = \ln k(M - 1 - k) \quad (12)$$

This reaches a maximum when k=0.5(M-1). This is the drawback of this property" [17].

"The entropy objective function is combined with the Otsu approach to construct a new objective function to solve this limitation by replacing W with φ (k)" [11].

$$T^{*} = \underset{0<k<M-1}{\arg\max}\{\varphi(k)(\omega_1(k)(\mu_1(k))^2 + \omega_2(k)(\mu_2(k))^2)\} \quad (13)$$

2.7. Postprocessing

The final phase in achieving the ultimate vessel segmentation result involves post-processing. Following the thresholding step, the resulting image may contain some unwanted noise. This noise can lead to the misclassification of isolated pixel clusters as vessels when they are, in fact, non-vessels. We employ a pixel-level thresholding technique to eliminate these non-vessel pixels. As per this study, the application of pixel-level thresholding is extended by setting specific pixel area thresholds: 10 for DRIVE datasets and 50 for STARE datasets. We categorize any pixel area equal to or lower than these predefined thresholds as a non-vessel pixel [19]. Following the removal of these non-vessel pixels, we arrive at the ultimate vessel segmented image. Fig. 5 displays the segmentation outcomes of two datasets.

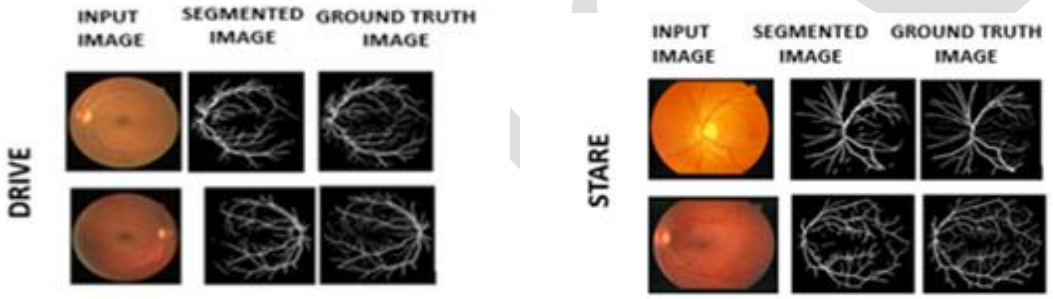

Fig. 5. Segmentation Outcomes Of DRIVE And STARE Datasets.

3. Results and Discussion

The research employed MATLAB R2018a software as a tool to design methods using computer equipment. The specifications used are the Intel(R) Core TM i5-7200U CPU @ 2.50 GHz, 2.70 GHz, 4.00 GB of memory, a 64-bit operating system, and an x64-based processor. To evaluate the efficacy of the retinal vasculature segmentation scheme, we utilized two freely accessible datasets, namely DRIVE and STARE. These datasets include manually annotated images for the entire dataset. The DRIVE dataset [20] consists of both testing and training sets, with each set containing 20 photographs. Within this comprehensive photograph collection, 7 photographs exhibit signs of initial stage diabetic retinopathy. Ground truth data is available for the testing set, enabling performance assessment. The STARE database [21] comprises 20 images, with 10 images depicting retinal pathology and the other 10 images representing healthy retinas. To estimate the efficiency of the suggested system, the resultant image after segmentation is compared with the reference image, providing a means to scrutinize its performance.

Three distinct mathematical metrics are utilized to evaluate performance, sensitivity (Sen) quantifies the segmentation approach's ability to correctly identify vessel pixels, specificity (Spec), on the other hand, assesses the

method's effectiveness in correctly identifying non-vessel pixels and Accuracy (Acc) measures how well the segmented image aligns with the reference image. The performance metric equation are shown in Table 3. The suggested approach was also compared with the current methodologies, described in both Table 4 and Table 5.

We compare our algorithm with recently developed methods, as shown in Table 4 and Table 5. Below, we highlight key observations from Table 4. Table 4 shows that the proposed method outperforms all other methods in terms of accuracy (Acc) on the DRIVE dataset. Moreover, the specificity (Spec) values of our developed algorithm are also much higher than a few of the compared techniques showed therein. Although published works report higher Sensitivity (Se) except in [29], it has less accuracy (Acc) than the proposed method. Table 5 reveals that the published works from [32] and [22] have reported higher accuracy on the STARE dataset.

On the STARE dataset, the works reported in [32], [22], and [28] yield higher specificity values than the proposed method. The proposed vessel segmentation algorithm yields the highest sensitivity of all the methods compared.

Table 3. Performance Metric Equations

Metrics	Equation
Sen	Sen = TP / (FN +TP)
Spec	Spec = TN / (FP + TN)
Acc	Acc= TN+TP / (FN+TN+FP+TP)

Table 4. Analyses of DRIVE Dataset Performance Using Various Methodologies

References	Year	Sen	Spec	Acc
[22]	2020	0.4346	0.9981	0.9478
[23]	2018	0.5582	0.9862	0.9537
[24]	2020	0.5978	0.9876	0.9532
[25]	2019	0.6129	0.9744	0.9431
[26]	2020	0.6326	0.9723	0.9371
[27]	2018	0.675	0.988	0.946
[28]	2018	0.6887	0.9765	0.9389
[29]	2020	0.6994	0.9811	0.945
[30]	2017	0.693	0.979	0.939
[31]	2023	0.6645	0.9697	0.9503
Presented Approach		0.6948	0.9814	0.9546

Table 5. Analyses of STARE Dataset Performance Using Various Methodologies

References	Year	Sen	Spec	Acc
[32]	2019	0.4317	0.9718	0.9488
[22]	2020	0.5557	0.9839	0.9441
[28]	2018	0.6801	0.9711	0.9388
[33]	2015	0.7019	0.9671	0.9189
[34]	2018	0.7116	0.9454	0.9231
Presented approach		0.7244	0.9653	0.9438

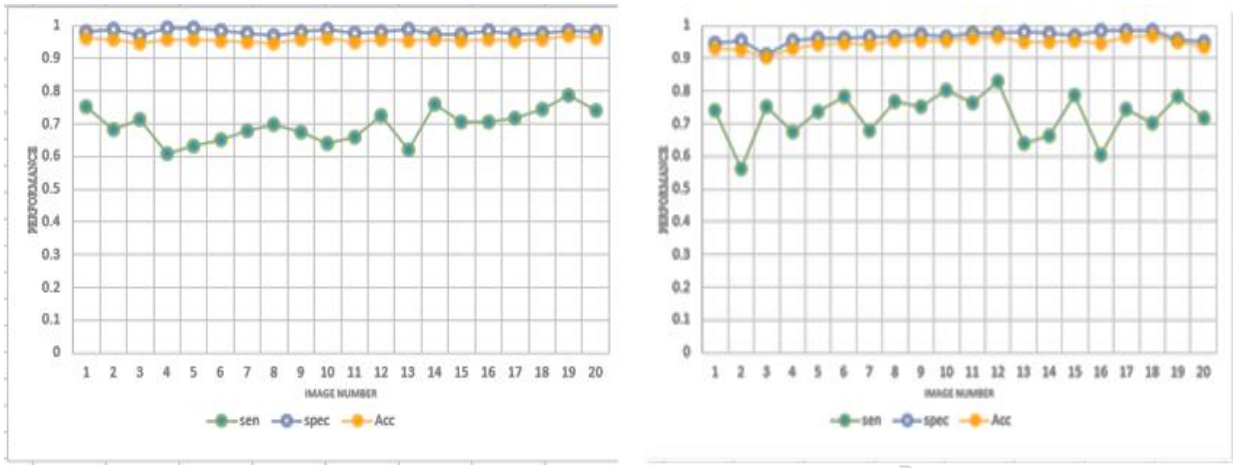

Fig. 6. Indicators of Performance Measurements of DRIVE and STARE Datasets.

4. Conclusıon

This paper introduces a method for extracting vascular structures in the retinal image based on Otsu entropy thresholding. We enhance the visibility of blood vessels by employing CLAHE and homomorphic filtering. The edges are preserved by using a bilateral filter. The residual image is then determined by subtracting bilateral filtered image from the homomorphic filtered image. After that, the background excluded image is obtained for further segmentation. The entire procedure is straightforward and requires minimal execution time. Our approach has demonstrated commendable performance, with a mean sensitivity, specificity, and accuracy of approximately, 0.6948, 0.9814, and 0.9546 with respect to the DRIVE dataset, and, 0.7244, 0.9653, and 0.9438 over the STARE dataset, respectively. The proposed scheme belongs to an unsupervised strategy. The key benefit of this approach is that it is quite simple and more feasible. The approach's drawback lies in the inaccurate detection of thin vessels and the presence of noise in certain images. In the future, we could focus on improving sensitivity. The developed algorithm could also be investigated for pathological cases, which experiences high false positive rates. Therefore, we can implement deep learning methods in the future to accurately detect both minor and thick vessels.

References

1. Radha, K., & Karuna, Y. (2023). Retinal vessel segmentation to diagnose diabetic retinopathy using fundus images: A survey. International Journal of Imaging Systems and Technology.
2. Franklin, S. W., & Rajan, S. E. (2014). Computerized screening of diabetic retinopathy employing blood vessel segmentation in retinal images. biocybernetics and biomedical engineering, 34(2), 117-124.
3. Marín, D., Aquino, A., Gegúndez-Arias, M. E., & Bravo, J. M. (2010). A new supervised method for blood vessel segmentation in retinal images by using gray-level and moment invariants-based features. IEEE Transactions on medical imaging, 30(1), 146-158.
4. Fraz, M. M., Remagnino, P., Hoppe, A., Uyyanonvara, B., Rudnicka, A. R., Owen, C. G., & Barman, S. A. (2012). An ensemble classification-based approach applied to retinal blood vessel segmentation. IEEE Transactions on Biomedical Engineering, 59(9), 2538–2548.
5. Xiao, Z., Adel, M., & Bourennane, S. (2013). Bayesian method with spatial constraint for retinal vessel segmentation. Computational and mathematical methods in medicine, 2013.

6. Roychowdhury, S., Koozekanani, D. D., &Parhi, K. K. (2015). Blood Vessel Segmentation of Fundus Images by Major Vessel Extraction and Sub image Classification. IEEE Journal of Biomedical and Health Informatics, 19(3), 1118–1128.
7. Zhu, C., Zou, B., Zhao, R., Cui, J., Duan, X., Chen, Z., & Liang, Y. (2017). Retinal vessel segmentation in colour fundus images using extreme learning machine. Computerized Medical Imaging and Graphics, 55, 68-77.
8. Orlando, J. I., Prokofyeva, E., &Blaschko, M. B. (2017). A discriminatively trained fully connected conditional random field model for blood vessel segmentation in fundus images. IEEE Transactions on Biomedical Engineering, 64(1), 16–27.
9. Memari, N., Ramli, A. R., Saripan, M. I. B., Mashohor, S., & Moghbel, M. (2017). Supervised retinal vessel segmentation from color fundus images based on matched filtering and AdaBoost classifier. PLoS One, 12(12), e0188939.
10. Chaudhuri, S., Chatterjee, S., Katz, N., Nelson, M., & Goldbaum, M. (1989). Detection of blood vessels in retinal images using two-dimensional matched filters. IEEE Transactions on medical imaging, 8(3), 263-269.
11. Maharana, D. K., Das, P., & Rout, R. K. (2023). Automated segmentation of blood vessels in retinal images based on entropy weighted thresholding. Computer Methods in Biomechanics and Biomedical Engineering: Imaging & Visualization, 11(3), 542-553.
12. Imani, E., Javidi, M., & Pourreza, H. R. (2015). Improvement of retinal blood vessel detection using morphological component analysis. Computer methods and programs in biomedicine, 118(3), 263-279.
13. Zhao, Y., Rada, L., Chen, K., Harding, S. P., & Zheng, Y. (2015). Automated vessel segmentation using infinite perimeter active contour model with hybrid region in formation with application to retinal images. IEEE transactions on medical imaging, 34(9), 1797-1807.
14. Dash, J., & Bhoi, N. (2018). An unsupervised approach for extraction of blood vessels from fundus images. Journal of digital imaging, 31, 857-868.
15. Saleh S. A. M., & Ibrahim H. (2012). Mathematical equations for homomorphic filtering in frequency domain: a literature survey. In proceedings of the international conference on information and knowledge management :74-77.
16. Tomasi, C., & Manduchi, R. (1998). Bilateral filtering for gray and color images: Proceedings of IEEE International Conference on Computer Vision.
17. Kapur JN, Sahoo PK, Wong AKC (1985) A new method for gray-level picture thresholding using entropy of the histogram. Comput. Vis. Graph. Image Process. 290 (3) :273-285.
18. Truong, M. T. N., & Kim, S. (2018). Automatic image thresholding using Otsu's method and entropy weighting scheme for surface defect detection. Soft Computing, 22, 4197-4203.
19. Fawcett, T. (2006). An introduction to ROC analysis. Pattern recognition letters, 27(8), 861-874.
20. Staal, J. J., Abràmoff, M. D., Niemeijer, M., Viergever, M. A., & van Ginneken, B. (2004). Ridge-based vessel segmentation in color images of the retina. IEEE Transactions on Medical Imaging, 23(4), 501–509.
21. Hoover, A. D., Kouznetsova, V., & Goldbaum, M. (2000). Locating blood vessels in retinal images by piecewise threshold probing of a matched filter response. IEEE Transactions on Medical imaging, 19(3), 203-210.
22. Erwin, Erwin & Damayanti, Heranti. (2020). Supervised Retinal Vessel Segmentation Based Average Filter and Iterative Self Organizing Data Analysis Technique. International Journal of Computational Intelligence

and Applications. 20. 2150003. 10.1142/S1469026821500036.

23. Mostafiz, T., Jarin, I., Fattah, S. A., & Shahnaz, C. (2018, December). Retinal blood vessel segmentation using residual block incorporated U-Net architecture and fuzzy inference system. In 2018 IEEE International WIE Conference on Electrical and Computer Engineering (WIECON-ECE) (pp. 106-109). IEEE.
24. Jadoon, Z., Ahmad, S., Jadoon, M. A. K., Imtiaz, A., Muhammad, N., & Mahmood, Z. (2020, January). Retinal blood vessels segmentation using ISODATA and high boost filter. In 2020 3rd International Conference on Computing, Mathematics and Engineering Technologies (iCoMET) (pp. 1-6). IEEE.
25. Pal S, Chatterjee S, Dey D, Munshi S (2019) Morphological operations with iterative rotation of structuring elements for segmentation of retinal vessel structures. Multidim Syst Sign Process,30(1):373–389.https://doi.org/10.1007/s11045-018-0561-9.
26. Khatter, K., Relan, D., & Mishra, A. (2020, December). Retinal Vessel Segmentation using Robinson Compass Mask and Fuzzy C-Means. In 2020 IEEE 17th India Council International Conference (INDICON) (pp. 1-6). IEEE.
27. Dash, J., Parida, P., & Bhoi, N. (2020). Retinal blood vessel extraction from fundus images using enhancement filtering and clustering. ELCVIA: electronic letters on computer vision and image analysis, 19(1), 0038-52.
28. Ben Abdallah, M., Azar, A. T., Guedri, H., Malek, J., & Belmabrouk, H. (2018). Noise-estimation-based anisotropic diffusion approach for retinal blood vessel segmentation. Neural Computing and Applications, 29, 159-180.
29. Adapa, D., Joseph Raj, A. N., Alisetti, S. N., Zhuang, Z., K, G., & Naik, G. (2020). A supervised blood vessel segmentation technique for digital Fundus images using Zernike Moment based features. Plos one, 15(3), e0229831.
30. Farokhian, F., Yang, C., Demirel, H., Wu, S., & Beheshti, I. (2017). Automatic parameters selection of Gabor filters with the imperialism competitive algorithm with application to retinal vessel segmentation. Biocybernetics and Biomedical Engineering, 37(1), 246-254.
31. Dash, S., Parida, P., & Sahu, G. (2023). An Enhanced Gabor Filter Based on Heat-Diffused Top Hat Transform for Retinal Blood Vessel Segmentation. In Advancements in Bio-Medical Image Processing and Authentication in Telemedicine (pp. 247-281). IGI Global.
32. AlSaeed, D., Bouridane, A., Jafri, R., Al-Ghreimil, N., Al-Baity, H. H., & Alhudhud, G. (2020). A novel blood vessel extraction using multiscale matched filters with local features and adaptive thresholding. Biosci. BioTechol. Res. Commun, 13, 1104-1113.
33. Vega, R., Sanchez-Ante, G., Falcon-Morales, L. E., Sossa, H., & Guevara, E. (2015). Retinal vessel extraction using lattice neural networks with dendritic processing. Computers in biology and medicine, 58, 20-30.
34. Aguirre-Ramos, H., Avina-Cervantes, J. G., Cruz-Aceves, I., Ruiz-Pinales, J., & Ledesma, S. (2018). Blood vessel segmentation in retinal fundus images using Gabor filters, fractional derivatives, and Expectation Maximization. Applied Mathematics and Computation, 339, 568-587.